JMB

Large Conformational Changes in the Maturation of a Simple RNA Virus, *Nudaurelia capensis* ω Virus (NωV)

Mary A. Canady[1], Mariana Tihova[2], Terry N. Hanzlik[3], John E. Johnson[1]* and Mark Yeager[1,2,4]*

[1]*Department of Molecular Biology and*

[2]*Department of Cell Biology The Scripps Research Institute 10550 N. Torrey Pines Rd La Jolla, CA 92037, USA*

[3]*Division of Entomology Box 1700, Canberra, ACT Australia*

[4]*Division of Cardiovascular Diseases, Scripps Clinic, 10666 N. Torrey Pines Rd, La Jolla CA 92037, USA*

*Corresponding authors

An assembly intermediate of a small, non-enveloped RNA virus has been discovered that exhibits striking differences from the mature virion. Virus-like particles (VLPs) of *Nudaurelia capensis* ω virus (NωV), a $T = 4$ icosahedral virus infecting Lepidoptera insects, were produced in insect cells using a baculovirus vector expressing the coat protein. A procapsid form was discovered when NωV VLPs were purified at neutral pH conditions. These VLPs were fragile and did not undergo the autoproteolytic maturation that occurs in the infectious virus. Electron cryo-microscopy (cryoEM) and image analysis showed that, compared with the native virion, the VLPs were 16 % larger in diameter, more rounded, porous, and contained an additional internal domain. Upon lowering the pH to 5.0, the VLP capsids became structurally indistinguishable from the authentic virion and the subunits autoproteolyzed. The NωV protein subunit coordinates, which were previously determined crystallographically, were modelled into the 28 Å resolution cryoEM map of the procapsid. The resulting pseudo-atomic model of the NωV procapsid demonstrated the large rearrangements in quaternary and tertiary structure needed for the maturation of the VLPs and presumably of the virus. Based on this model, we propose that electrostatically driven rearrangements of interior helical regions are responsible for the large conformational change. These results are surprising because large structural rearrangements have not been found in the maturation of any other small RNA viruses. However, similarities of this conformational change to the maturational processes of more complex DNA viruses (e.g. bacteriophages and herpesvirus) and to the swelling of simple plant viruses suggest that structural changes in icosahedral viruses, which are integral to their function, have similar strategies and perhaps mechanisms.

© 2000 Academic Press

Keywords: conformational change; tetravirus; pseudo-atomic; virus assembly; modelling

Introduction

In the life-cycles of viruses, dramatic morphological changes in their capsid structure are needed to allow them to carry out the diverse set of functions required for replication. All virus capsids must form readily, have structural integrity, and have the proper biological trigger in order to be infectious. It is clear that complex viruses undergo multi-stage assembly that is orchestrated by protein-protein and/or protein-nucleic acid interactions. The most dramatic and best characterized of these changes occur in the double-stranded DNA (dsDNA) bacteriophages, where structural intermediates can often be characterized at low resolution (Prasad *et al.*, 1993). The dsDNA herpes simplex virus undergoes a maturational transition that is comparable to that of the dsDNA bacterio-
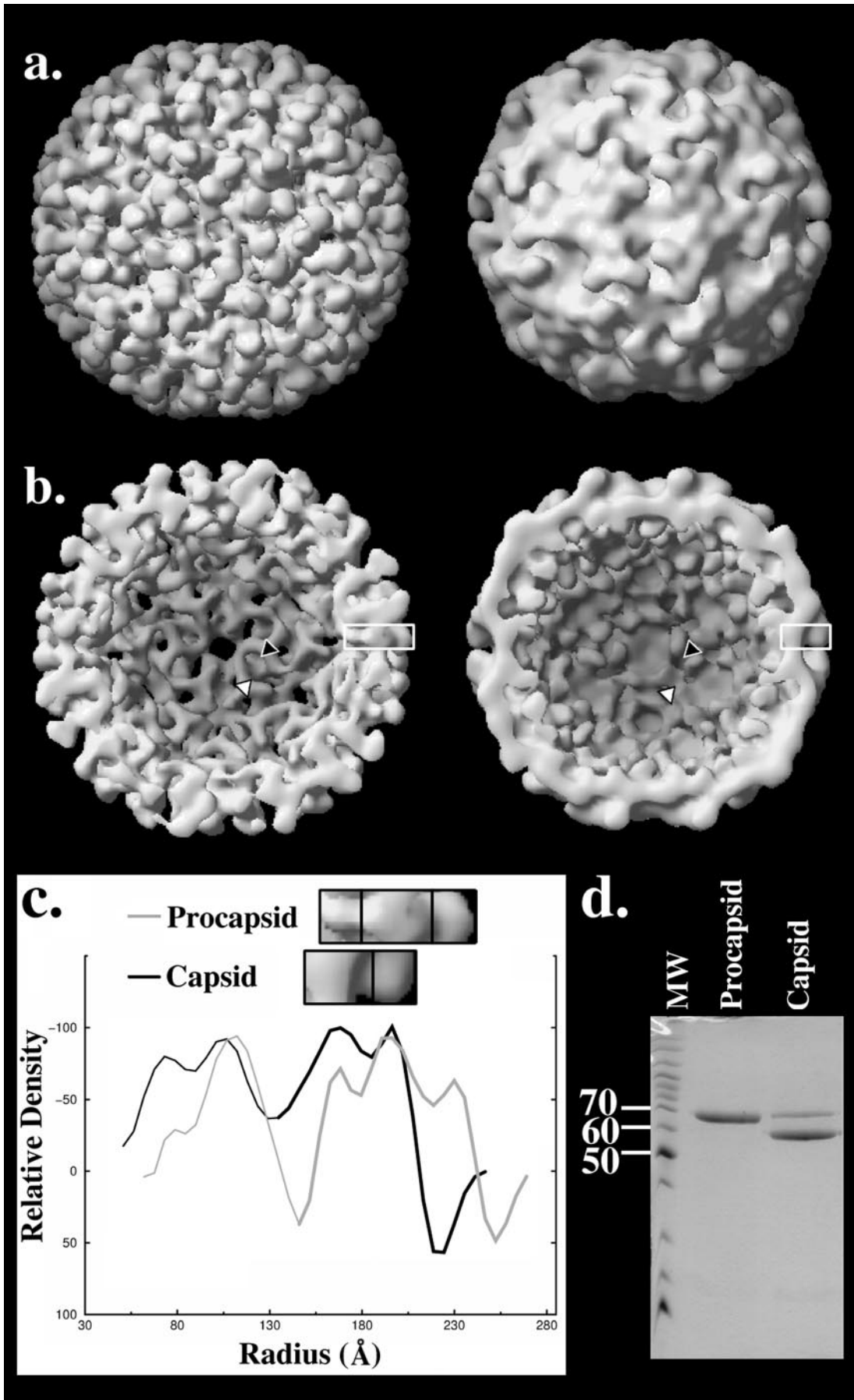
Figure 1 (*legend opposite*)

phages (Trus et al., 1996). In both cases a rounded precursor matures into a polyhedral capsid. Many other large structural changes have been described in the assembly and maturation of complex RNA and DNA viruses, both enveloped and non-enveloped (Allison et al., 1995; Andres et al., 1998; Edvardsson et al., 1976; Salanueva et al., 1999; Turner & Summers, 1999). The molecular interactions that trigger these structural transitions are not well understood, in part because no atomic resolution model is available for the assembly intermediates. By combining the crystallographic model of Nudaurelia capensis ω virus (NωV) with the structure of the procapsid obtained using electron cryomicroscopy (cryoEM), we have been able to model a viral assembly intermediate for the first time.

NωV is a $T = 4$, icosahedral, single-stranded RNA virus that belongs to the tetravirus family, whose members infect insects of the lepidopteran order (Murphy et al., 1995). The viral capsids assemble from 240 copies of the 70 kDa coat protein, which adopt four slightly different conformations in the capsid (designated A, B, C, and D) according to the theory of quasiequivalence (Caspar & Klug, 1962). After assembly, all of the subunits are cleaved autocatalytically, resulting in 62 kDa (β) and 8 kDa (γ) products (Agrawal & Johnson, 1992). A similar phenomenon occurs in the $T = 3$ insect nodaviruses, where autoproteo-

Figure 1. Three-dimensional, surface-shaded (a) full particle and (b) sectioned views of the procapsid (left) and capsid (right) of NωV VLPs viewed down a 2-fold symmetry axis, with 3-fold (black triangle) and quasi 3-fold (white triangle) axes marked in (b). The procapsid is larger, rounded, and porous, while the mature capsid has a smaller, angular, solid shell. (c) The radial density plots reveal that the capsid protein shell (black line) spanned 62 Å with two domains, whereas the procapsid (gray line) had a thickness of 83 Å and comprised three domains. A cross-section of each map is shown above the plot, the domains delineated and placed in register with the radii to which they correspond. (d) An SDS-PAGE gel showing that the procapsid sample contains the 70 kDa uncleaved coat protein, while the capsid contains mostly 62 kDa and 8 kDa (not visible) coat protein fragments which result from autoproteolysis upon lowering of the pH to 5.0. The recombinant baculovirus expressing the NωV coat protein was made from the pFBWCap plasmid using the bacmid reagents supplied by BRL. The pFBWCap plasmid was made by inserting a blunt-ended RT-PCR product of the NωV coat protein into the StuI site of the plasmid, pFastBac (BRL). The PCR product was obtained by performing 12 PCR cycles (20-95 °C, 20-55 °C, 4-70 °C) with Pfu polymerase (Stratagene) upon cDNA made with SuperScript II (BRL) and RNA extracted from NωV purified on a CsCl density gradient (kindly supplied by Don Hendry). The primers were designed using the NωV RNA2 sequence (Agrawal & Johnson, 1995) and were the phosphorylated primers W21 (GCAGCAAAACTGTCGTGTG), complementary to bases 2398-2416, and WcapN (GGAGATGGACAGTAACTCAGCC), complementary to bases 267-285. Four bases prior to the initiating ATG of the coat protein in WcapN were inserted in order to improve expression because baculovirus constructs having the endogenous context of the NωV coat protein ATG failed to give good expression. Spodoptera frugiperda (Sf21) cells were grown in TC-100 medium supplemented with 10 % (v/v) fetal bovine serum. Cells were infected as monolayers using a multiplicity of infection of 5. After incubation for four to five days at 27 °C, the cells were harvested, lysed with 0.5 % (v/v) NP40, and the virus-like particles (VLPs) were isolated by ultracentrifugation at 100,000 **g** through a 30 % (w/v) sucrose cushion. The pellets were resuspended overnight in buffer A (250 mM NaCl, 50 mM Tris (pH 7.5)). Debris was removed by low-speed centrifugation, and supernatant containing the procapsid VLPs was layered onto a 10 %-40 % (w/v) sucrose gradient in buffer A. After ultracentrifugation at 113,000 **g** for 2.5 hours, the band containing the VLPs was collected and dialyzed against buffer A, and then concentrated to 1-3 mg/ml. Mature capsids were obtained by diluting the procapsids 1:10 with buffer B (70 mM sodium acetate (pH 5.0)). Aliquots (∼4 µl) of virus suspension (∼1-2 mg/ml) were applied to holey carbon films on 400-mesh copper grids, blotted for ca four seconds with preheated filter paper, and then immediately plunged into liquid ethane. A Philips CM120 transmission electron microscope equipped with Gatan 626 cryo-specimen holder was used to record low-dose (5 to 10 electrons/Å^2) images at a magnification of 45,000× that were underfocussed by 0.8 to 1.2 µm. Optical diffraction was used to select images that displayed minimal astigmatism and drift based on the Thon rings in the contrast transfer function. Selected images were digitized at a 25 µm interval using a Perkin-Elmer microdensitometer, corresponding to 5.6 Å on the specimen. The program X3D (Conway et al., 1997) was used to extract particle images with a circular mask and subtract background density. An initial set of origin and orientation values for particles from a single micrograph were determined using cross-correlation and common line procedures (Baker et al., 1988; Crowther, 1971; Fuller, 1987; Olson & Baker, 1989). To optimize the search procedure, calculations were performed using only a portion of the Fourier transform of the masked image (between 1/70 Å and 1/35 Å). The published map of NωV at 28 Å resolution (Johnson et al., 1994) was used as the starting model for the polar Fourier transform (PFT) method (Baker & Cheng, 1996). The search procedure was optimized by using particle radii spanning the capsid shell. Some five to six cycles of refinement were performed using 1.0° increments, followed by six to eight cycles using 0.5° increments. During the latter refinement cycles, additional particles were progressively included and the resolution was extended from 35 to 20 Å. The final reconstructions of the procapsid and capsid were based on 57 and 259 particles, respectively. The final reconstruction of the authentic virion (not shown) was based on 46 particles and had a resolution limit of 25 Å. To assess the resolution of the maps, each data set was divided in half to compute two independent reconstructions at higher resolution. The program EMMAP3DT was used to generate a list of structure factors, and the program EMCTF03 used these data to compute the correlation coefficient as a function of spatial frequency by comparing the structure factors of the two independent reconstructions. All surface-shaded representations were visualized using AVS software (Upson et al., 1989). Contour levels were chosen to include the volume occupied by the capsid shell calculated from the number of copies and the molecular mass of the coat protein.
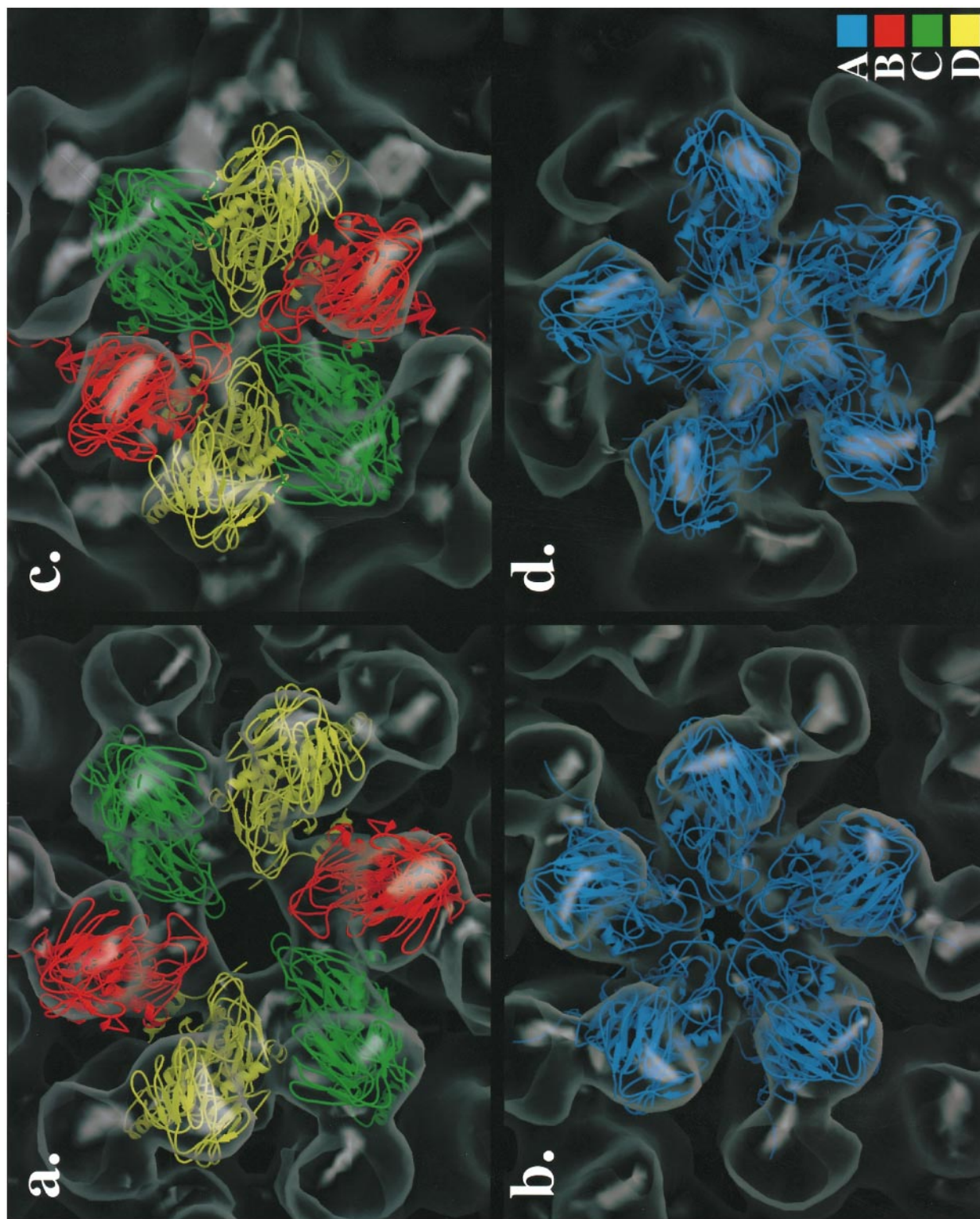
Figure 2 (*legend opposite*)

lysis is required for infectivity (Schneemann *et al.*, 1992). Although NωV shares little sequence homology with the nodaviruses, the 2.8 Å crystal structure of NωV showed that the subunit structures had similar β-sandwich folds, but that the NωV subunits have an immunoglobulin-like (Ig-like) domain protruding from the surface of the virus (Munshi *et al.*, 1996). The autoproteolytic active sites are superimposable, both having similarly placed ''γ peptide'' helices that are cleaved from the rest of the protein during the autoproteolysis. The placement of these α-helices in bundles interior to the 5-fold axes led to the prediction that they are involved in RNA delivery (Cheng *et al.*, 1994; Munshi *et al.*, 1996). Analogously, VP4 of the $T = 3$ picornaviruses is cleaved from the polyprotein and has been implicated in the delivery of the viral genome during infection (Rueckert, 1996).

Via a baculovirus vector, the 70 kDa NωV subunit was expressed in Sf21 insect cells, and the gene product spontaneously formed virus-like particles (VLPs) containing heterologous cellular RNA. These VLPs were readily purified at pH 7.5, but did not undergo autoproteolytic maturation (Figure 1(d)). Negative stain electron microscopy showed that the VLPs were fragile and structurally distinct from authentic virions. Lowering the pH to 5.0 resulted in more robust VLPs that resembled authentic virions. Additionally, the coat protein α was cleaved into β (1-570) and γ (571-644) peptides. Solution X-ray scattering revealed that the structural transition occurred within seconds (data not shown), while the autoproteolytic cleavage required hours for completion. We designate the immature VLP as a procapsid because it is a structurally distinct precursor of the biologically relevant capsid form of the virus which does not allow maturation to take place. The biological relevance of procapsids isolated from VLP systems has recently been substantiated by the finding that the herpes simplex virus procapsid discovered *in vitro* was also identified in infected cells (Newcomb *et al.*, 2000).

The structures of the procapsid, capsid, and authentic virion (indistinguishable from capsid at 25 Å resolution; data not shown here) were determined using cryoEM and image reconstruction (Figure 1). While the procapsid has a round shape and an external radius of 240 Å, the capsid has a polyhedral shape and a smaller radius of 210 Å (Figure 1(c)). The appearance of the two particles differs greatly because the Ig-like domains form conspicuous dumbbell-shaped dimers on the exterior of the procapsid while they are trimeric in the capsid, resulting in a smoother surface (Figure 1(a)). The capsid shell is solid, but the procapsid is perforated by holes at all of the symmetry axes (Figure 1(a) and (b)), the smallest present at the 5-fold axes (Figure 2(b)). The quasi-hexamers, composed of two each of the B, C, and D subunits, are slightly distorted, causing the holes at the quasi 6-fold axes to be ellipsoidal (Figure 2(a)). This distortion is notable because it has been described at the quasi 6-fold axes in bacteriophage (Conway *et al.*, 1995; Dokland & Murialdo, 1993; Prasad *et al.*, 1993) and herpesvirus procapsids (Newcomb *et al.*, 1996). In all cases, the symmetry is restored to near 6-fold symmetry in the mature capsid.

The radial density plots derived from the cryoEM data (Figure 1(c)) revealed an additional internal domain in the procapsid. The mature capsid has density corresponding to two domains centered at radii of 160 Å (shell) and 200 Å (Ig-like), whereas the procapsid has density corresponding to three domains, centered at radii of 160 (internal), 190 Å (shell) and 230 Å (Ig-like). The internal domain of the procapsid is triskelion-shaped and found on the inner surface at both the 3-fold (DDD trimer) and quasi 3-fold (ABC trimer) axes (Figures 1(b) and 4(a)).

To delineate the subunit rearrangements as the procapsid form matures to the capsid, the NωV X-ray coordinates were fitted into the procapsid cryoEM density (Figure 2(a) and (b)). An *R*-value of 45 % was obtained after rigid body refinement using the entire subunit as a fixed body. This

Figure 2. The fit of the color-coded (key shown on right), quasiequivalent NωV subunits (Munshi *et al.*, 1996) into the cryoEM density of the (a), (b) procapsid and (c), (d) capsid. Exterior views down the (a) quasi 6-fold and (b) 5-fold axes of the procapsid reveal a good fit with the Ig-like and shell domains. (c) and (d) The same views of the unaltered crystallographically determined (Munshi *et al.*, 1996) positions are shown within the capsid cryoEM map. The X-ray coordinates of NωV (Munshi *et al.*, 1996) were fitted into the cryoEM maps using the program O (Jones *et al.*, 1991). Because the Ig-like domains were the most recognizable feature in the map, they were used as a starting point. Additionally, the disposition of the domains was very similar to their disposition in the CD dimer, so these domains were ''excised'' from the subunits and fitted to both the AB and CD external domain densities. Once a reasonable fit had been obtained, each subunit was superimposed, based on the position of the fitted Ig-like domain. Minor adjustments were then made, moving the subunits as rigid bodies, with the exception of the C subunit, where the best fit was obtained when the shell and the Ig-like domains were moved independently of one another. Structure factors between 300 and 30 Å resolution were calculated from the cryoEM map using the CCP4 program package (Collaborative Computational Project, 1994). Using the X-PLOR package (Brünger, 1996); 100 cycles of rigid body refinement were performed for each trial. The final positions of the subunits were analyzed using polyhedral models of the subunits, which were drawn using the O descriptor language and then rendered using Raster3D (Merritt & Bacon, 1997). The Figure was generated using BobScript (Esnouf, 1997; Kraulis, 1991) and Raster3D (Merritt & Bacon, 1997).
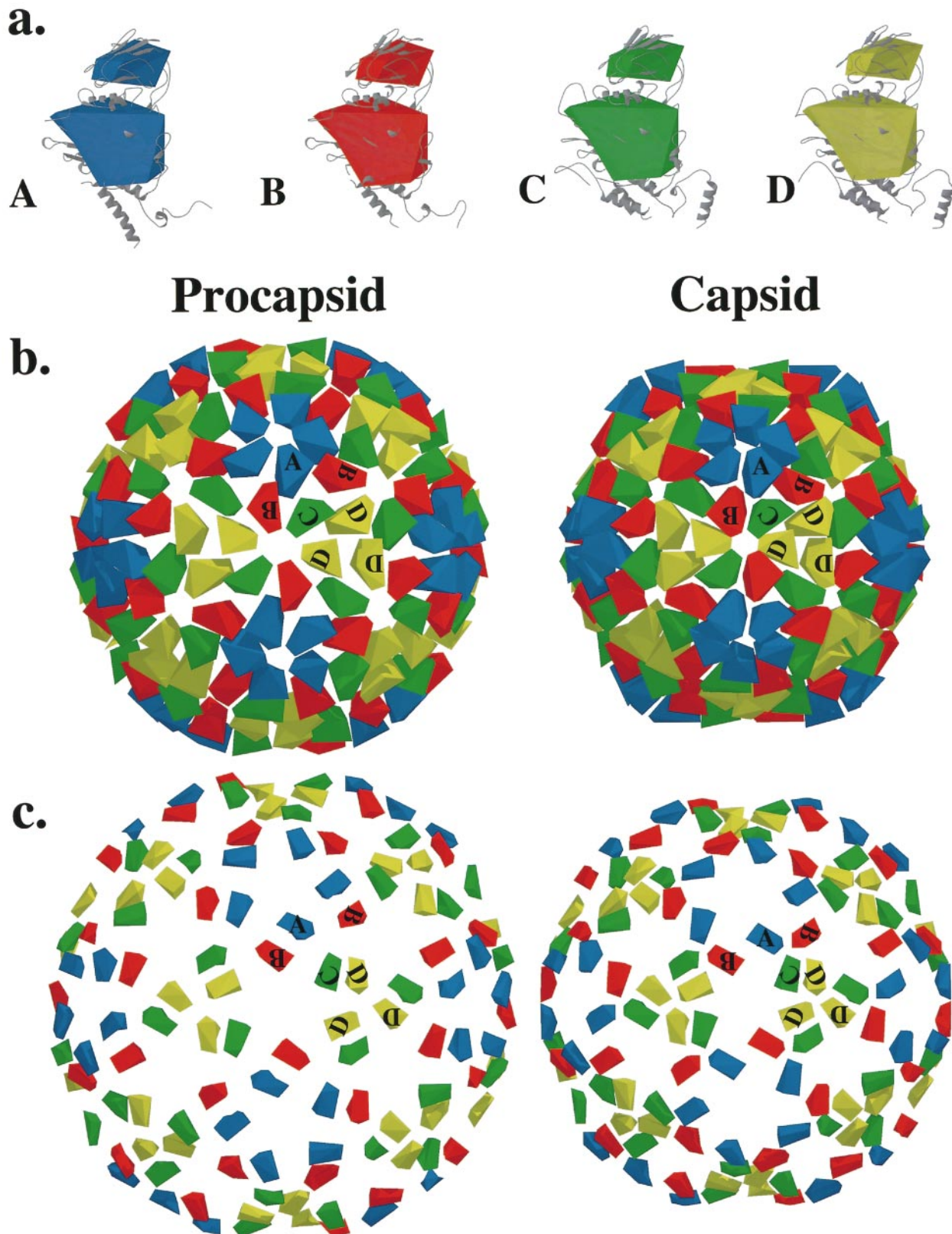
Figure 3. The procapsid and capsid models depicted using (a) polyhedra placed in the positions of the protein sub-unit (b), shell domains and (c) Ig-like domains. (b) In the procapsid pseudo-atomic model, the shell domains are radially equidistant, oriented similarly, and AB and CD dimeric interactions dominate. In the capsid atomic model, the A subunits are tilted and positioned further from the center than the other subunits, thereby forming the vertices of the icosahedron, and trimeric (ABC and DDD) interactions dominate. (c) The dimeric (procapsid) and trimeric (capsid) quaternary arrangement is more evident in the Ig-like domains because the axes of rotation for the A and B subunits passes through the shell domains roughly tangential to the shell, causing the shell domain to act as a ''fulcrum'' during the rotation of the subunit.

R-value was comparable to that determined in the control experiment, using the unmodified X-ray coordinates and the cryoEM map of the capsid. The procapsid model *R*-value improved only slightly when the shell and Ig-like domains were refined as independent units. Thus, the conformational change primarily involves rigid body movements of the subunits without significant hinging between the Ig and shell domains. The resulting pseudo-atomic model of the procapsid was then used to qualitatively examine the transition with the aid of simplified models of the crystallographic subunits (Figure 3(a)). These models simplified the structures of the shell and Ig-like domains, leaving out the internal domains because they are present only in the procapsid and are thus not easily modelled using the capsid subunits. Analysis of these models revealed that the AB and CD dimers dominate the procapsid while the capsid is dominated by ABC and DDD trimers. However, inspection of the interior of the procapsid (Figures 1(b) and 4(a)) shows that the internal domains behave almost conversely: they are obviously trimeric in the procapsid, and in the capsid they lose these associations and become less distinct as domains (Figure 4(b)).

All four subunits translate towards the center of the particle during the transition, and the A and B subunits also undergo a significant rotation. The A/B and C/D dimers are roughly equivalent in the procapsid, and both contribute equally to the curvature of the rounded particle. The rotation of the A and B subunits during the transition causes them to differentiate from the C/D dimer, leading to a ''bent'' contact present between the facets of the polyhedral capsid. The description of the subunit interactions in the NωV procapsid is very similar to that of the *T* = 3 plant virus cowpea chlorotic mottle virus (CCMV) (Speir *et al.*, 1995); namely, equivalent dimers both contributing to the curvature of the capsid. This so-called truncated icosahedral geometry is distinct from the canonical icosahedral geometry, where a ''molecular switch'' (Johnson, 1996) differentiates the two types of dimers in the capsid.

While the movements of the subunits using the pseudoatomic model explain the procapsid to capsid transition, it is likely that the conformational change originates from a rearrangement of the procapsid internal domain. The crystallographically visible N and C termini are interior to the capsid shell, so the internal domain is probably comprised of N and C-terminal regions that are significantly rearranged from their dispositions in the capsid. The internal structure of the procapsid suggests that the internal domain stabilizes the procapsid and determines its curvature, and significant alterations in this domain would be needed for the procapsid to condense into the smaller, polyhedral capsid (Figure 4). Similarly, the curvature of the hepatitis B core is determined by a positively charged C-terminal region (Zlotnick *et al.*, 1996). That the N and C-terminal regions would be involved in the conformational change follows logically from the discussion of the geometrical change described above. In the truncated icosahedron, all subunits have nearly equivalent structures, and this is seen especially in the internal domain of the procapsid, where the density at the 3-fold and quasi 3-fold axes is closely similar (Figure 1(b)). In the icosahedron, however, the quasi-symmetry is compromised by the molecular switch which is formed in the capsid by the N and C termini (Munshi *et al.*, 1996), thus requiring a conformational change in this region.

In the NωV capsid structure, the A and B subunits have less ordered structure at their N and C termini. In the C and D subunits, these ordered fragments are α-helical and can be found along the quasi 2-fold axes between C and D in the capsid. We believe that in the procapsid, all four subunits have comparable secondary structure with the capsid C and D subunits, and that these α-helices comprise the procapsid internal domain (Figure 4(c)). During the procapsid to capsid conformational change, we propose the N and C-terminal α- helices lose their trimeric associations at the quasi 3-fold and 3-fold axes and then reside at the quasi 2-fold axes. Additionally, for the A and B subunits, some α-helical regions (residues 44-57 and 600-644) either become disordered or no longer conform to icosahedral symmetry. In the polyhedral capsid structure there is less room for these α-helices at the ''bent'' quasi 2-fold axes between and internal to the A and B subunits. A similar situation has been described in the structure of swollen tomato bushy stunt virus (TBSV), where the A and B subunits are thought to have more ordered, interior structures than in the unswollen form (Robinson & Harrison, 1982). Both tertiary (movement of α-helices) and perhaps secondary (disordering of α-helices) structural changes are implicated in the NωV conformational change. Similarly, maturation of the bacteriophage P22 procapsid is thought to involve tertiary structural changes in the coat protein which result in stronger quaternary interactions (Tuma *et al.*, 1998).

The atomic interactions responsible for the conformational change are not yet clear because of the significant rearrangement that occurs during the transition and the lack of a high-resolution structure of the NωV procapsid. At this resolution, we can expect that the pseudo-atomic model of the procapsid could be used along with biochemical data to suggest groups of residues or regions of the coat protein that may be involved in the conformational change, but not for a detailed description of specific atomic interactions responsible. The transition described here occurs in an all-or-none fashion when the pH is reduced from 7.6 to 5.0, but X-ray solution scattering demonstrated that initial changes in structure occur if the pH is reduced to ∼6.0 (data not shown). Therefore, we assume that the transition is caused by side-chain(s) which become protonated at pH 6.0,
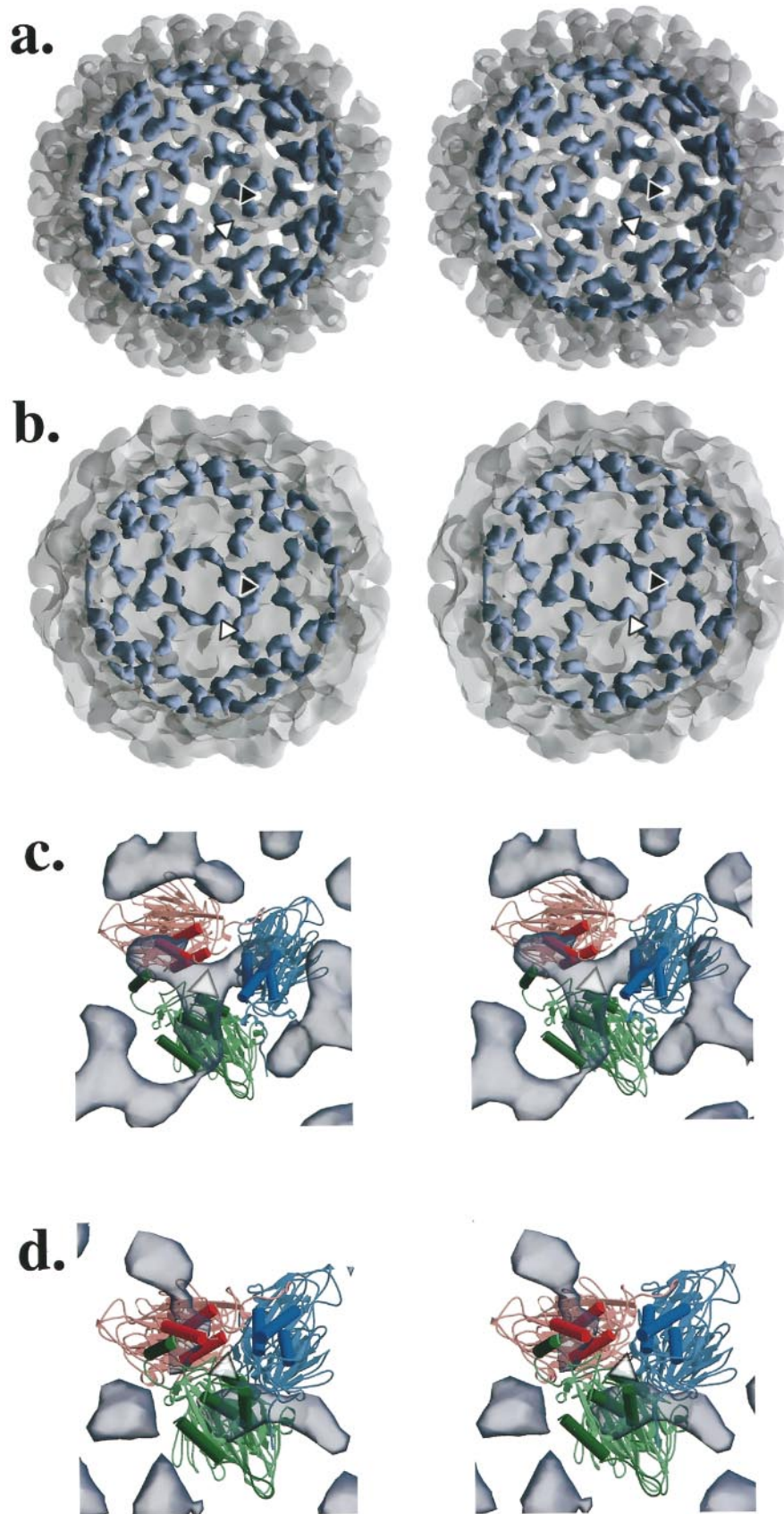
Figure 4 (*legend opposite*)

causing the repulsion and/or attraction required for rearrangement of the internal domain. A histidine residue is an obvious choice for protonation in this pH range, but is absent from the N and C-terminal regions. Analogies can be made to the swelling of plant viruses which occurs when the pH is raised. Mechanisms for expansion of TBSV (Robinson & Harrison, 1982) and CCMV (Speir et al., 1995) are thought to involve aspartic acid side-chains present at the quasi 3-fold axes which normally bind calcium ions. When the pH is raised in the presence of EDTA, repulsion of negatively charged carboxyl groups causes swelling of the capsid. The transition takes place above neutral pH, and it is thought that the pK_a values of these side-chains must be anomalously high due to their environment. Similar electrostatic repulsion may be important for maintaining the NωV procapsid. It is also conceivable that arginine residues, which are abundant in the N and C termini, might have anomalously low pK_a values (as has been observed for lysine residues (Kokesh & Westheimer, 1971)), becoming charged at pH 6.0 and causing the dissolution of the trimeric internal domain due to electrostatic repulsion. Electrostatic interactions have also been implicated in the scaffolding/coat protein interactions in the maturation of bacteriophage P22 (Parker & Prevelige, 1998), and the region of the scaffolding protein thought to be involved is a helix-loop-helix domain with a region that is rich in positive charges.

It appears that the rearrangement of the internal domain would be completed before the autoproteolysis in the capsid would begin, although further rearrangement could occur as the autoproteolysis proceeds. The autoproteolytic active site is found in each subunit at the interface between the 5-fold (A) and quasi 6-fold (B, C, D) related subunits. The reaction is thought to be catalyzed by the intrasubunit Glu103 (Munshi et al., 1996), by direct analogy to the nodaviruses where site-directed mutagenesis showed that the corresponding residue (Asp75) is required for the reaction (Zlotnick et al., 1994). For the nodaviruses, a structurally distinct procapsid form has not been observed, and intersubunit interactions are thought to allow cleavage to occur only in the fully assembled capsid. This intersubunit "communication" is less clear in the structure of the NωV capsid. The fact that significant rearrangement of the internal domain occurs during maturation suggests that this rearrangement, rather than intersubunit communication, may be sufficient for activating autoproteolysis in NωV.

Our results extend the familiar theme of the initial formation of a round precursor particle which matures into a biologically functional polyhedral form from the well-established complex DNA virus systems to a simple RNA virus. The phenomenon can now be understood as a mechanism for viral subunits to assemble as nearly equivalent units, which then differentiate only after assembly has completed (Figure 5). The round shape, while it facilitates assembly, has compromised stability. The fact that many viral cores (hepatitis (Böttcher et al., 1997; Conway et al., 1997), Sindbis (Paredes et al., 1993), bluetongue virus VP3 (Grimes et al., 1998)) are round substantiates this idea, since these shells are protected by an outer layer and appear to have been evolutionarily optimized for ease of assembly rather than for independent structural integrity. Our study supports the idea that round viral cores and assembly intermediates in fact have truncated icosahedral geometry (Speir et al., 1995), which explains both their more rounded appearance and their nearly equivalent subunits (Wynne et al., 1999). The NωV procapsid internal domain, which is "lost" as the capsid is formed, can be seen as a functional equivalent of scaffolding proteins in bacteriophage, which physically leave the capsid upon maturation.

Parallels with complex and simpler viruses can also be made concerning the quaternary rearrangements seen in the NωV procapsid to capsid transition. The switching of the subunit interactions from dimeric to trimeric has been seen in the low pH-induced maturation of tick-borne encephalitis virus (TBE) (Allison et al., 1995). It is also notable that the swollen forms of plant viruses exhibit dimeric interactions which appear more equivalent and stronger than in the unswollen capsid (Speir et al., 1995; Robinson & Harrison, 1982). Many plant viruses are thought to assemble from dimers (Choi & Loesch-Fries, 1999; Sorger et al., 1986; Rossmann et al., 1983), and recently the hepatitis core has been shown to assemble from dimers of the coat protein (Zlotnick et al., 1999). By analogy to the NωV assembly intermediate observed here, it is tempting to speculate that when plant viruses

Figure 4. The procapsid internal triskelion domain has a less obvious organization in the capsid. (a) Cutaway view of the procapsid (as shown in Figure 1(b), now semi-transparent) with the internal triskelion domain shown in purple. (b) The same view of the capsid with the innermost regions (now no longer a distinct domain) colored purple. (c) View of these domains from the interior of the procapsid at the quasi 3-fold axis showing the A, B, and C subunits of the pseudo-atomic model (crystallographically determined subunits fitted to the cryoEM density). The N and C-terminal helices thought to be involved in the conformational change are shown as rods. The breakdown of the 3-fold symmetry in the crystallographic subunits is noticeable (compared with the symmetry they must possess in the procapsid), as well as the absence of trimeric interactions in the pseudo-atomic model, which obviously are present in the cryoEM density. (d) The same view as in (c) of the capsid. AVS (Upson et al., 1989) was used to generate (a) and (b), and BobScript (Esnouf, 1997) was used for (c) and (d).

NωV Subunits Differentiate Late in Virus Assembly

In Solution: **During Assembly:**   **In Procapsid:**

Monomers → **Identical Dimers** → **Nearly Identical Dimers** →

Capsid Begins to Form: **Mature Capsid:**
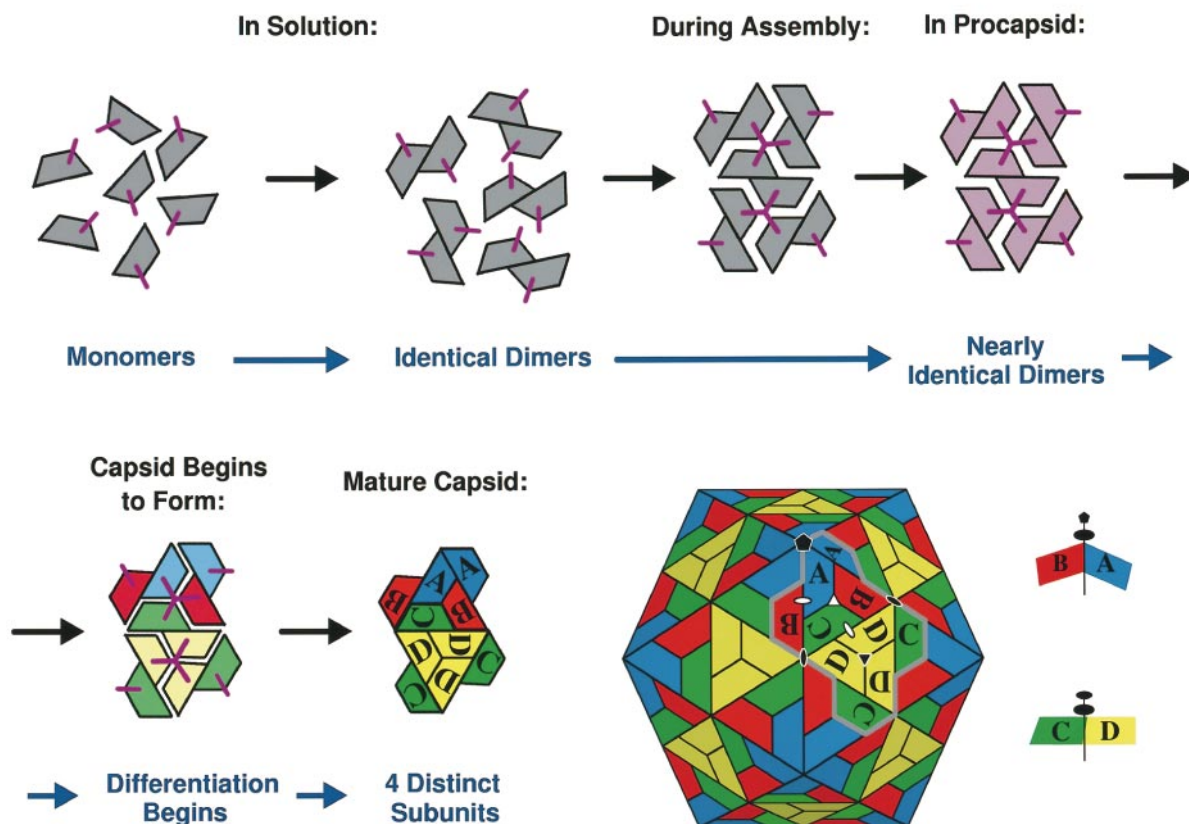
→ **Differentiation Begins** → **4 Distinct Subunits**

Figure 5. Schematic of the assembly of NωV based on the structure of the procapsid assembly intermediate. Dimers (gray) are assumed to be the building blocks of assembly, due to their tight associations in the procapsid. Because every dimer exists in the non-differentiating milieu of the cytoplasm, we can assume that they are identical. The dimers form associations with other dimers *via* their N and C-terminal regions, which form the trimeric internal domain (purple lines which become triskelions; shown external to the procapsid for clarity). The dimers remain closely similar in the procapsid, but may have become altered slightly from their structure in solution (denoted by a change in color from gray to purple). As the procapsid shrinks and the capsid begins to form, the subunits differentiate as they adjust to their slightly different environments, the endpoint being the four distinct subunits present in the $T = 4$ polyhedral capsid (shown schematically, lower right). In the mature capsid, the internal domain has become the molecular switch which differentiates the AB and CD dimers (shown to the right of the $T = 4$ icosahedron).

swell, they are reverting to a previously formed assembly intermediate. The lack of observable swollen forms in $T = 3$ animal viruses such as picornaviruses may be precluded by their proteolytic maturation, which may stabilize them and be a reflection on their different means of infection.

The pseudo-atomic model of the NωV procapsid presented here demonstrates the extreme versatility of the viral coat protein. The structure of the coat protein that initially assembles is surprisingly different from that of the mature viral subunit, resulting in a dramatically different quaternary arrangement in the NωV procapsid, causing it to exhibit very different structural properties from the mature capsid. The mostly dimeric procapsid matures into the trimeric capsid by putative electrostatic interactions in the trimeric internal domain, which eventually lead to its disappearance as a distinct domain. The similarities of this system to both more complex and simpler viruses suggests that similar strategies are used by many viruses irrespective of their complexity to form a stable capsid.

References

Agrawal, D. K. & Johnson, J. E. (1992). Sequence and analysis of the capsid protein of *Nudaurelia capensis* ω Virus, an insect virus with $T = 4$ icosahedral symmetry. *Virology,* **190**, 806-814.

Agrawal, D. K. & Johnson, J. E. (1995). Assembly of the $T = 4$ *Nudaurelia capensis* ω virus capsid protein, post-translational cleavage, and specific encapsidation of its mRNA in a baculovirus expression system. *Virology,* **207**, 89-97.

Allison, S. L., Schalich, J., Stiasny, K., Mandl, C. W., Kunz, C. & Heinz, F. X. (1995). Oligomeric rearrangement of tick-borne encephalitis virus envelope proteins induced by an acidic pH. *J. Virol.* **69**, 695-700.

Andrés, G., García-Escudero, R., Simón-Mateo, C. & Viñuela, E. (1998). African swine fever virus is enveloped by a two-membraned collapsed cisterna derived from the endoplasmic reticulum. *J. Virol.* **72**, 8988-9001.

Baker, T. S. & Cheng, R. H. (1996). A model-based approach for determining orientations of biological macromolecules imaged by cryoelectron microscopy. *J. Struct. Biol.* **116**, 120-130.

Baker, T. S., Drak, J. & Bina, M. (1988). Reconstruction of the three-dimensional structure of simian virus 40 and visualization of the chromatin core. *Proc. Natl Acad. Sci. USA,* **85**, 422-426.

Böttcher, B., Wynne, S. A. & Crowther, R. A. (1997). Determination of the fold of the core protein of hepatitis B virus by electron cryomicroscopy. *Nature,* **386**, 88-91.

Brünger, A. T. (1996). Recent developments for crystallographic refinement of macromolecules. *Methods Mol. Biol.* **56**, 245-266.

Caspar, D. L. D. & Klug, A. (1962). Physical principles in the construction of regular viruses. *Cold Spring Harbor Symp. Quant. Biol.* **27**, 1-24.

Cheng, R. H., Reddy, V. S., Olson, N. H., Fisher, A. J., Baker, T. S. & Johnson, J. E. (1994). Functional implications of quasi-equivalence in a $T = 3$ icosahedral animal virus established by cryo-electron microscopy and X-ray crystallography. *Structure,* **2**, 271-282.

Choi, J. & Loesch-Fries, L. S. (1999). Effect of C-terminal mutations of alfalfa mosaic virus coat protein on dimer formation and assembly *in vitro*. *Virology,* **260**, 182-189.

Collaborative Computational Project, No. 4 (1994). The CCP4 suite: programs for protein crystallography. *Acta Crystallog. sect. D,* **50**, 760-763.

Conway, J. F., Duda, R. L., Cheng, N., Hendrix, R. W. & Steven, A. C. (1995). Proteolytic and conformational control of virus capsid maturation: the bacteriophage HK97 system. *J. Mol. Biol.* **253**, 86-99.

Conway, J. F., Cheng, N., Zlotnick, A., Wingfield, P. T., Stahl, S. J. & Steven, A. C. (1997). Visualization of a 4-helix bundle in the hepatitis B virus capsid by cryo-electron microscopy. *Nature,* **386**, 91-94.

Crowther, R. A. (1971). Procedures for three-dimensional reconstruction of spherical viruses by Fourier synthesis from electron micrographs. *Phil. Trans. Roy. Soc. ser. B,* **261**, 221-230.

Dokland, T. & Murialdo, H. (1993). Structural transitions during maturation of bacteriophage lambda capsids. *J. Mol. Biol.* **233**, 682-694.

Edvardsson, B., Everitt, E., Jörnvall, H., Prage, L. & Philipson, L. (1976). Intermediates in adenovirus assembly. *J. Virol.* **19**, 533-547.

Esnouf, R. M. (1997). An extensively modified version of MolScript that includes greatly enhanced coloring capabilities. *J. Mol. Graph. Model.* **15**, 132-134, 112-113 color plates.

Fuller, S. D. (1987). The $T = 4$ envelope of Sindbis virus is organized by interactions with a complementary $T = 3$ capsid. *Cell,* **48**, 923-934.

Grimes, J. M., Burroughs, J. N., Gouet, P., Diprose, J. M., Malby, R., Ziéntara, S., Mertens, P. P. C. & Stuart, D. I. (1998). The atomic structure of the bluetongue virus core. *Nature,* **395**, 470-478.

Johnson, J. E. (1996). Functional implications of protein-protein interactions in icosahedral viruses. *Proc. Natl Acad. Sci. USA,* **93**, 27-33.

Johnson, J. E., Munshi, S., Liljas, L., Agrawal, D., Olson, N. H., Reddy, V., Fisher, A., McKinney, B., Schmidt, T. & Baker, T. S. (1994). Comparative studies of $T = 3$ and $T = 4$ icosahedral RNA insect viruses. *Arch. Virol. Suppl.* **9**, 497-512.

Jones, T. A., Zou, J.-Y., Cowan, S. W. & Kjeldgaard, M. (1991). Improved methods for building protein models in electron density maps and the location of errors in these models. *Acta Crystallog. sect. A,* **47**, 110-119.

Kokesh, F. C. & Westheimer, F. H. (1971). A reporter group at the active site of acetoacetate decarboxylase. II. Ionization constant of the amino group. *J. Am. Chem. Soc.* **93**, 7270-7274.

Kraulis, P. J. (1991). MOLSCRIPT: a program to produce both detailed and schematic plots of protein structures. *J. Appl. Crystallog.* **24**, 946-950.

Merritt, E. A. & Bacon, D. J. (1997). Raster3D: photorealistic molecular graphics. *Methods Enzymol.* **277**, 505-524.

Munshi, S., Liljas, L., Cavarelli, J., Bomu, W., McKinney, B., Reddy, V. & Johnson, J. E. (1996). The 2.8 Å structure of a $T = 4$ animal virus and its implications for membrane translocation of RNA. *J. Mol. Biol.* **261**, 1-10.

Murphy, F. A., Fauquet, C. M., Bishop, D. H. L., Ghabrial, S. A., Jarvis, A. W., Martelli, G. P., Mayo, M. A. & Summers, M. D. (1995). Editors of *Virus Taxonomy: Classification and Nomenclature of Viruses. The Sixth Report of the International Committee on Taxonomy of Viruses*, Springer-Verlag, Wíen.

Newcomb, W. W., Homa, F. L., Thomsen, D. R., Booy, F. P., Trus, B. L., Steven, A. C., Spencer, J. V. & Brown, J. C. (1996). Assembly of the herpes simplex virus capsid: characterization of intermediates observed during cell-free capsid formation. *J. Mol. Biol.* **263**, 432-446.

Newcomb, W. W., Trus, B. L., Cheng, N., Steven, A. C., Sheaffer, A. K., Tenney, D. J., Weller, S. K. & Brown, J. C. (2000). Isolation of herpes simplex virus procapsids from cells infected with a protease-deficient mutant virus. *J. Virol.* **74**, 1663-1673.

Olson, N. H. & Baker, T. S. (1989). Magnification calibration and the determination of spherical virus diameters using cryo-microscopy. *Ultramicroscopy,* **30**, 281-297.

Paredes, A. M., Brown, D. T., Rothnagel, R., Chiu, W., Schoepp, R. J., Johnston, R. E. & Prasad, B. V. (1993). Three-dimensional structure of a membrane-containing virus. *Proc. Natl Acad. Sci. USA,* **90**, 9095-9099.

Parker, M. H. & Prevelige, P. E., Jr (1998). Electrostatic interactions drive scaffolding/coat protein binding and procapsid maturation in bacteriophage P22. *Virology,* **250**, 337-349.

Prasad, B. V. V., Prevelige, P. E., Marietta, E., Chen, R. O., Thomas, D., King, J. & Chiu, W. (1993). Three-dimensional transformation of capsids associated with genome packaging in a bacterial virus. *J. Mol. Biol.* **231**, 65-74.

Robinson, I. K. & Harrison, S. C. (1982). Structure of the expanded state of tomato bushy stunt virus. *Nature,* **297**, 563-568.

Rossmann, M. G., Abad-Zapatero, C., Hermodson, M. A. & Erickson, J. W. (1983). Subunit interactions in southern bean mosaic virus. *J. Mol. Biol.* **166**, 37-73.

Rueckert, R. R. (1996). Picornaviridae: the viruses and their replication. In *Fields Virology* (Fields, B. N., Knipe, D. N., Howley, P. M., Chanock, R. M., Melnick, J. L., Monath, T. P., Roizman, B. & Straus, S. E., eds), 3rd edit., pp. 609-654, Lippincott-Raven Publishers, Philadelphia.

Salanueva, I. J., Carrascosa, J. L. & Risco, C. (1999). Structural maturation of the transmissible gastroenteritis coronavirus. *J. Virol.* **73**, 7952-7964.

Schneemann, A., Zhong, W., Gallagher, T. M. & Rueckert, R. R. (1992). Maturation cleavage required for infectivity of a nodavirus. *J. Virol.* **66**, 6728-6734.

Sorger, P. K., Stockley, P. G. & Harrison, S. C. (1986). Structure and assembly of turnip crinkle virus. II. Mechanism of reassembly *in vitro*. *J. Mol. Biol.* **191**, 639-658.

Speir, J. A., Munshi, S., Wang, G., Baker, T. S. & Johnson, J. E. (1995). Structures of the native and swollen forms of cowpea chlorotic mottle virus determined by X-ray crystallography and cryo-electron microscopy. *Structure,* **3**, 63-78.

Trus, B. L., Booy, F. P., Newcomb, W. W., Brown, J. C., Homa, F. L., Thomsen, D. R. & Steven, A. C. (1996). The herpes simplex virus procapsid: structure, conformational changes upon maturation, and roles of the triplex proteins VP19c and VP23 in assembly. *J. Mol. Biol.* **263**, 447-462.

Tuma, R., Prevelige, P. E., Jr & Thomas, G. J., Jr (1998). Mechanism of capsid maturation in a double-stranded DNA virus. *Proc. Natl Acad. Sci. USA,* **95**, 9885-9890.

Turner, B. G. & Summers, M. F. (1999). Structural biology of HIV. *J. Mol. Biol.* **285**, 1-32.

Upson, C., Faulhaber, T., Jr, Kamins, D., Laidlaw, D., Schlegel, D., Vroom, J., Gurwitz, R. & van Dam, A. (1989). The application visualization system: a computational environment for scientific visualization. *IEEE Comput. Graph. Applic.* **9**, 30-42.

Wynne, S. A., Crowther, R. A. & Leslie, A. G. W. (1999). The crystal structure of the human hepatitis B virus capsid. *Mol. Cell,* **3**, 771-780.

Zlotnick, A., Reddy, V. S., Dasgupta, R., Schneemann, A., Ray, W. J., Jr, Rueckert, R. R. & Johnson, J. E. (1994). Capsid assembly in a family of animal viruses primes an autoproteolytic maturation that depends on a single aspartic acid residue. *J. Biol. Chem.* **269**, 13680-13684.

Zlotnick, A., Cheng, N., Conway, J. F., Booy, F. P., Steven, A. C., Stahl, S. J. & Wingfield, P. T. (1996). Dimorphism of hepatitis B virus capsids is strongly influenced by the C terminus of the capsid protein. *Biochemistry,* **35**, 7412-7421.

Zlotnick, A., Johnson, J. M., Wingfield, P. W., Stahl, S. J. & Endres, D. (1999). A theoretical model successfully identifies features of hepatitis B virus capsid assembly. *Biochemistry,* **38**, 14644-14652.

Edited by D. Rees